Nanoscale

Hybrid vanadate waveguiding configurations for extreme optical confinement and efficient polarization management in the 'near-infrared'

Journal:	*Nanoscale*
Manuscript ID	NR-ART-06-2018-004982.R1
Article Type:	Paper
Date Submitted by the Author:	12-Aug-2018

Complete List of Authors:	Bian, Yusheng; Pennsylvania State University, Kang, Lei; Penn State Ren, Qiang; Beihang University Zheng, Yuanxia; Penn State Engel-Herbert, Roman; Penn State Werner, Ping; Penn State Werner, Douglas H.; Penn State Jacob, Ajey; Globalfoundries Inc Malta Thomas, Abu; Globalfoundries Inc Malta

Hybrid vanadate waveguiding configurations for extreme optical confinement and efficient polarization management in the near-infrared

Yusheng Bian[1,2], Lei Kang[1], Qiang Ren[3], Yuanxia Zheng[5,6], Roman Engel-Herbert[4,5,7], Pingjuan L. Werner[1], Douglas H. Werner[1,5]*, Ajey P. Jacob[2] and Abu Thomas[2]

[1]Computational Electromagnetics and Antennas Research Lab (CEARL)

Department of Electrical Engineering, The Pennsylvania State University

University Park, PA, 16802, USA

[2]Globalfoundries, 400 Stone Break Rd Extension, Malta, NY 12020, USA

[3]School of Electronics and Information Engineering, Beihang University

Beijing 100191, China

[4]Department of Materials Science and Engineering, The Pennsylvania State University

University Park, PA 16802, USA

[5]Materials Research Institute, The Pennsylvania State University

University Park, PA 16802, USA

[6]Department of Physics, The Pennsylvania State University

University Park, PA 16802, USA

[7]Department of Chemistry, The Pennsylvania State University

University Park, PA 16802, USA

**Corresponding Author. Email:dhw@psu.edu*

Abstract

Vanadate materials such as $CaVO_3$ and $SrVO_3$ were recently proposed as promising alternatives to their conventional transparent conducting oxide counterparts owing to the superior capability for simultaneous realization of high optical transparency and high electrical conductivity originating from strong electron-electron interactions. Here we show that, in addition to their remarkable optoelectronic properties as conducting materials, their incorporation into planar waveguiding configurations could enable outstanding optical performance that is otherwise difficult to achieve with conventional material building blocks, especially metals. Starting from the guided wave at a single $CaVO_3$/dielectric interface, the unique dispersion relationship and propagation property of the fundamental mode are revealed and compared with the conventional surface plasmon polariton associated with a silver/dielectric planar configuration. The superior confinement capability and the unique modal attenuation of the $CaVO_3$-based waveguiding platform are further demonstrated via investigating silicon-based hybrid guiding schemes integrated with a $CaVO_3$ nanostructure. By leveraging the pronounced polarization dependent loss in the hybrid configuration, an ultra-compact TE-pass polarizer is numerically demonstrated at telecommunication wavelengths. This transformative design features a reduced footprint and enhanced optical performance when benchmarked against the current state-of-the-art in hybrid silicon polarizers. The combination of these vanadate materials with traditional waveguiding platforms thereby opens new avenues towards miniaturized functional integrated photonic devices, and potentially enables a variety of intriguing applications at the sub-diffraction-limited scale.

Key words: Polarizer; Hybrid waveguides; Vanadate; Transparent conducting material; Silicon-on-insulator; Polarization dependent loss

1. **Introduction**

The ability to efficiently manage the propagation of light is of critical importance to the properties of integrated photonic systems as well as being vital to the manipulation of light-matter interactions [1, 2]. Featuring a compact configuration and tight optical confinement, silicon photonic and plasmonic structures, among others, have been identified as promising technologies for the realization of ultra-compact photonic waveguides, functional devices and high-density photonic integrated circuits [3-7]. In particular, plasmonics, with the potential to break the fundamental diffraction limit, provides a pathway towards the realization of numerous subwavelength components with unprecedented functionalities [8]. Although remarkable advancement has been made in this field within the past two decades [9], there is still an imminent need for better photonic components with a miniaturized foot-print and enhanced optical performance in order to satisfy the ever increasing demand for high-bandwidth, low-power-consumption global data communications [10].

One particularly promising direction that could greatly impact the field of plasmonics is to incorporate advanced materials into the system to enhance the guiding properties and realize disruptive functionalities. The substitution of novel materials for conventional metals such as gold and silver, could not only provide the possibility to modify the device performance, but also offer advantages in design flexibility, component reconfigurability and system integration [11]. Among the wide variety of

alternative materials being studied, including conventional semiconductors, perovskite oxides, metal nitrides, silicides, germanides, and 2D material such as graphene, transparent conducting oxides (TCOs) have been proposed as promising alternatives to gold and silver in the near-infrared regime [12-14]. In contrast to the well-explored application fields such as photovoltaics, displays, smart windows and solid-state lighting [15-18], the exploitation of TCOs as feasible waveguiding candidates and building blocks for functional photonic components has not attracted considerable attention until the past decade [19]. By changing the carrier concentration/doping, the optical properties of TCOs can be dynamically tuned, thereby enabling important applications in high-performance active devices such as modulators and switches [11, 20, 21]. Moreover, TCOs can be grown into thin films and other complex nanostructures, making them ideal candidates for a variety of different optical applications.

In addition to exploring various emerging application areas, remarkable advances have also been achieved in the discovery and characterization of new TCOs [22]. Vanadates ($CaVO_3$, $SrVO_3$, etc.), which are capable of satisfying the competing demands of high optical transparency and high electrical conductivity in the visible spectrum, have been identified quite recently as promising alternatives to their conventional TCO counterparts such as indium tin oxide (ITO) [23]. Interestingly, in contrast to noble metals, the real permittivity values of $CaVO_3$ and $SrVO_3$ are significantly smaller in magnitude [23], which potentially makes them appealing material building blocks for many photonic devices. Here in this paper, we explore, for the first time, the possibility of creating waveguiding structures and functional photonic components using these alternative conducting materials. We will show that, in addition to their remarkable opto-electronic properties as demonstrated before, the incorporation

of vanadate films and nanostructured elements in planar photonic waveguides can also lead to interesting guiding properties that are otherwise difficult to achieve with existing metals. In the following, besides analyzing the dispersion of the typical guided modes at a vanadate/dielectric interface, detailed comparisons are also made with that of surface plasmon polaritons (SPPs) bound to a single metal/dielectric configuration. In addition, by investigating the performance of hybrid composites that incorporate $CaVO_3$ substrates and other nanostructures, the superior confinement capability and unique propagation properties are further revealed. To demonstrate their potential in creating high-performance photonic devices, an ultra-compact TE-pass polarizer is developed based on a hybrid $CaVO_3$ platform operating at the telecommunication wavelengths. Its outstanding optical performance is revealed in detail and benchmarked against a state-of-the-art hybrid silicon polarizer.

2. Waveguiding properties of $CaVO_3$/dielectric interfaces and hybrid $CaVO_3$ composites

We start our investigation by considering the guided modes that can be supported at a $CaVO_3$/dielectric interface. It is worth mentioning that although $CaVO_3$ has been exclusively considered in our case study, a number of other vanadate materials can also be leveraged to realize similar functionalities. For instance, $SrVO_3$, which features quite similar optical properties at near-infrared frequencies as opposed to $CaVO_3$ [23], can be employed to build photonic waveguides and devices with comparable optical performance. In the following study, the fundamental modes existed in two types of 1D guiding configurations, including $CaVO_3$/air and $CaVO_3$/silica, are considered. Their optical properties are benchmarked against those of SPPs that are supported by a conventional Ag/dielectric interface. Note that the dispersion curves of the modes

supported by other two-layer systems, such as gold/dielectric, $SrVO_3$/dielectric and ITO/dielectric, are also plotted and compared in the Supplementary Information. In the calculations, the permittivity of $CaVO_3$ is extracted from room-temperature spectroscopic ellipsometry measurements (S1 of the Supplementary Information), whereas the model in [24] is adopted to describe the permittivity of Ag by fitting its parameters to experimental data from the literature [25]. For all the considered configurations, the guiding properties are investigated by employing the full-vectorial eigenmode solver of COMSOL Multiphysics, which is a finite element method (FEM) based software package. Convergence tests are conducted to ensure that the numerical boundaries and meshing do not interfere with the solutions.

The dispersion relations of the fundamental modes supported by the four considered 1D configurations are shown in Fig. 1 (a). For reference, the dispersion curves for the vacuum and silica light lines are also included. Clearly, the SPP modes guided by the Ag/dielectric configurations exhibit no cutoff within the considered frequency range, with both dispersion curves (*i.e.* the orange and green curves) lying outside the shaded area bounded by the dispersion relation of the vacuum light line. In sharp contrast to the waveguides involving Ag, the guided modes in the $CaVO_3$/dielectric structures exhibit significantly different dispersion behavior at optical and near-infrared frequencies (*i.e.* the red and blue curves). The wave vectors of the modes in the $CaVO_3$/air and $CaVO_3$/silica structures are significantly greater than their corresponding SPP counterparts at longer wavelengths (*e.g.* > 1.2 μm), while asymptotically approaching the vacuum and silica light lines when the wavelength becomes shorter. As the operational wavelength shifts towards the optical regime, non-monotonic trends can be observed in the dispersion curves of the $CaVO_3$-based configurations (*e.g.* 0.9 ~ 1.2 μm),

leading to dramatically reduced wave vectors that are even shorter than those of the SPPs and light lines. These unique dispersion characteristics arise from the transition between different modes, where a gradual conversion from the bound mode, to the quasi-bound and radiative modes occurs with increasing energy (See S2 of the Supplementary Information for details). The complex dispersion relation observed in the near-infrared regime for the $CaVO_3$-based modes closely resembles the behavior of SPP waves propagating along an Ag/dielectric interface at near-ultraviolet frequencies [24]. The considerably larger wave vectors of the $CaVO_3$-based guided modes in the near-infrared also reflect the superior confinement capability of the waveguides, which will be discussed further by investigating other modal parameters. It is worth mentioning here that the Ag-based SPP modes feature even stronger optical confinement in the near-ultraviolet regime than their vanadate counterparts (See S2 of the Supplementary Information). However, due to the fact that such behavior only occurs at high optical frequencies, vanadate materials are more suitable candidates for specific applications in the optical communication bands, *e.g.* as building blocks for data centers and telecommunications networks.

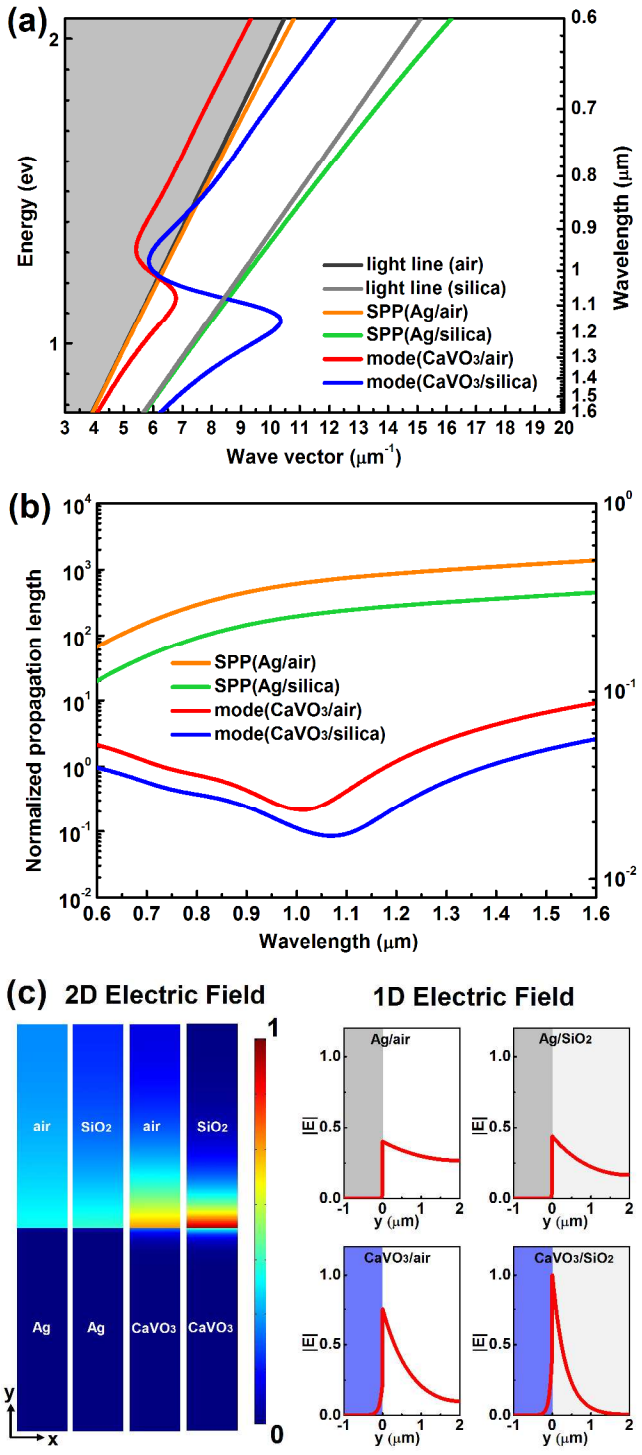

Fig. 1. (a) Dispersion relations of the fundamental guided modes at $CaVO_3$/air and $CaVO_3$/silica interfaces. The dispersion curves of the SPP modes supported by Ag/air and Ag/silica interfaces are plotted as well to allow for direct comparisons. (b) Normalized propagation lengths of the modes as

a function of the working wavelength. (c) 2D and 1D normalized electric field distributions of the guided fundamental modes for different configurations at the wavelength of 1.55 μm.

In order to gain a deeper understanding of the modal behavior, we next study the propagation lengths of the guided modes. The normalized propagation length (L/λ), shown in Fig. 1 (b), is obtained by calculating the ratio between the propagation length ($L = \lambda/[4\pi\mathrm{Im}(N_{eff})]$) and its operating wavelength (λ), where N_{eff} is the complex modal effective index. As clearly illustrated in the figure, the propagation distances of the guided SPP modes at an Ag/air (silica) interface demonstrate monotonic increases when the wavelength becomes larger. In contrast, owing to the transition between different modes, non-monotonic behavior is observed for propagation lengths of the $CaVO_3$-based geometries. Another distinct feature is that the propagation distances of the modes supported by the $CaVO_3$/air (silica) interfaces are more than one order of magnitude smaller than those of the corresponding SPP waves. Such limited propagation lengths indicate the significantly high attenuation rates of the guided modes associated with the $CaVO_3$ material system.

To further demonstrate the confinement capability of $CaVO_3$ waveguides, 2D and 1D electric field distributions of the fundamental modes guided by the Ag/air (silica) and $CaVO_3$/air (silica) structures at the wavelength of 1.55 μm are depicted in Fig. 1 (c). A close examination reveals that significantly more pronounced local field enhancement can be enabled at the $CaVO_3$/dielectric interfaces as opposed to the Ag-based structures. In addition, the penetration depths of the guided waves in the $CaVO_3$-based configurations are considerably larger than their SPP counterparts, leading to stronger interactions between the mode field and the lossy $CaVO_3$ substrate. Calculations of the confinement factor, defined as the ratio of the power inside the considered region to the

total power of the waveguide, reveal that the proportions of the power that resides inside the $CaVO_3$ substrate is more than two orders of magnitude larger than those in Ag for both cases. The significantly larger confinement factors result in much higher modal attenuations, and consequently, dramatically shortened propagation distances as seen in Fig. 1 (b). The unique optical properties of the guided modes associated with $CaVO_3$/dielectric interfaces could potentially provide the ability to develop advanced photonic devices with unique optical performance that would be otherwise difficult to realize with existing material building blocks.

Hybrid plasmonic waveguides, which integrate plasmonic configurations and high-index dielectric structures, have attracted considerable research interest during recent years owing to their superior capability for highly-efficient light transmission at the sub-diffraction-limited scale [26-29]. Here we further explore the optical waveguiding properties of a hybrid configuration that incorporates a $CaVO_3$ substrate, and compare its performance to that of a conventional hybrid waveguide employing Ag. Since the fundamental hybrid mode originates from the coupling between the bound mode at the $CaVO_3$/dielectric interface and the photonic waveguiding mode, to a certain degree its optical properties share similarities to those of the 1D $CaVO_3$ mode. Fig. 2 shows the normalized electric field distributions of the fundamental modes supported by two typical hybrid configurations. For both waveguides, the width (height) of the silicon ridge is chosen as 200 nm and the size of the silica gap is set to be 10 nm. As expected, the $CaVO_3$-based hybrid waveguide enables significantly more pronounced local field enhancement inside the nanoscale gap region as compared to its Ag-based counterpart. The observation of the electric field tails that spread out into the $CaVO_3$ substrate is a clear indication of a large penetration depth, which further enhances the interactions of

the optical field with the substrate, leading to dramatically increased modal attenuation. Quantitative calculations of the modal parameters confirm the superior confinement capability and the lossy feature of the hybrid $CaVO_3$ mode. Results indicate that the power ratio inside the silica gap of the hybrid $CaVO_3$ waveguide is nearly twice as large as that of the Ag-based hybrid structure. Moreover, the proportion of the mode power inside the $CaVO_3$ substrate reaches 21%, which is over 46 times greater than that in Ag. The significant mode portion in the lossy $CaVO_3$ substrate results in a surprisingly high imaginary part of the complex modal effective index (*i.e.* 0.54*i), which is more than two orders of magnitude larger than that of the Ag-based hybrid mode. Furthermore, the real part of the complex modal effective index of the CaVO3 fundamental mode is also substantially higher than that of the Ag-based structure ($\Delta n_{eff} > 1.26$), indicating greatly enhanced field confinement.

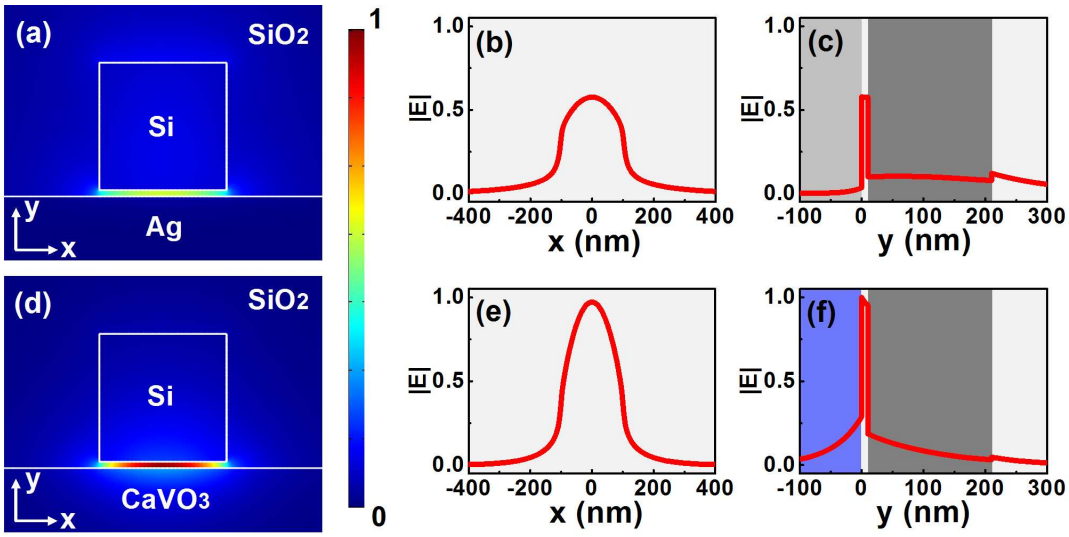

Fig. 2. Normalized electric field distributions of the fundamental hybrid modes: (a)-(c) conventional Ag-based hybridized waveguide; (d)-(e) modified hybrid configuration with a $CaVO_3$ substrate. Both structures consist of a rectangular silicon ridge separated from the substrate by a nanoscale silica gap. Both modes are analyzed at the telecommunication wavelength of 1.55 μm.

Since silicon-based hybrid plasmonic waveguides allow seamless integration with standard silicon photonic platforms and offer a practical route torward realistic functional devices [20, 30], we further investigate the properties of the guided modes in a hybrid configuration that consists of a $CaVO_3$ nanowire located above a silica-coated silicon ridge waveguide, as shown schematically in Fig. 3 (a). Here, the waveguide dimensions are chosen as w = 500 nm, h = 220 nm, $w_1 = h_1$ = 200 nm, W = 900 nm and H = 420 nm. Results indicate that, with the presence of the $CaVO_3$ nanowire, the losses of the modes in the hybrid configuration are highly polarization dependent: the quasi-TE mode features an ultra-low-loss and a high modal effective index due to the substantial modal overlap with the silicon ridge and low overlap with the $CaVO_3$ nanowire (Fig.3 (b)), whereas both the fundamental and higher-order quasi-TM modes are extremely lossy owing to the significantly enhanced interaction with the lossy $CaVO_3$ region (Figs. 3 (c)-(d)). Such a pronounced loss contrast between the TE and TM modes can be leveraged to create ultra-compact, highly-efficient polarization handling devices such as polarizers, as will be shown in the next section.

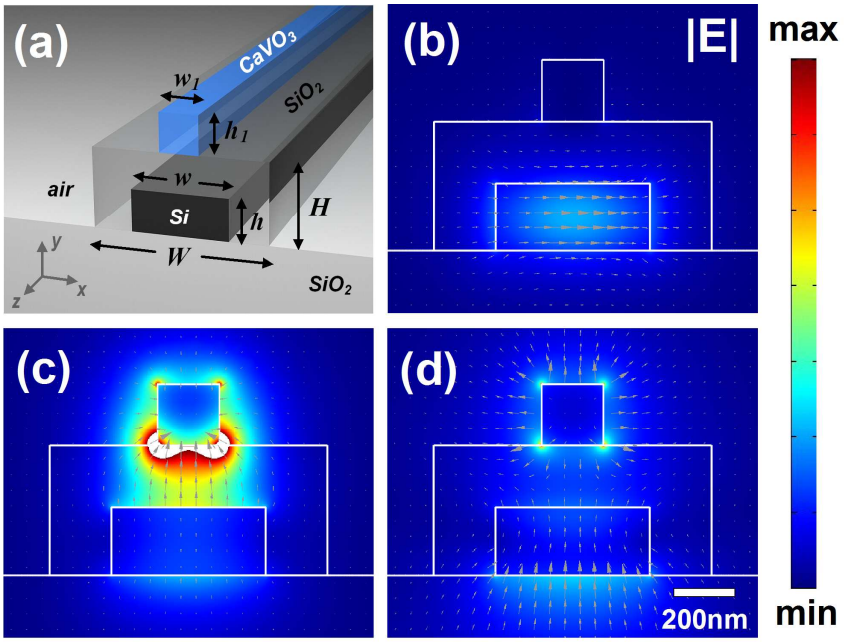

Fig. 3. (a) Sketch of the silicon-based hybrid $CaVO_3$ waveguide, comprised of a $CaVO_3$ nanowire placed on top of a silica-coated silicon ridge waveguide. (b)-(d) Electric field distributions of the quasi-TE, fundamental and higher-order quasi-TM modes in a typical configuration operating at 1.55 μm. Arrows in the 2D field profiles indicate the orientations of the electric fields.

3. Ultra-compact TE-pass polarizer enabled by a silicon-based hybrid $CaVO_3$ waveguide

The ability to precisely manage the polarization state of light is vital to maintaining the high performance of advanced optical systems, especially for those involving high-index-contrast silicon photonic components that are extremely polarization dependent [31-33]. Introducing a polarization diversity scheme into the system, for example, represents a feasible route toward polarization-transparent circuits, yet such a strategy inevitably adds significant complexities to the system, while resulting in a considerably increased device footprint. Another commonly adopted, simpler and cost-effective approach is to utilize an optical polarizer to extinguish the unwanted polarization state. Recently, a significant amount of attention has been devoted to this field, leading to a

wide variety of compact, silicon-on-insulator (SOI)-compatible integrated polarizers [34-39]. For instance, a 1 mm-long TE-pass polarizer based on shallowly etched SOI waveguides was shown to enable an extinction ratio of 25 dB over a 100 nm wavelength range [34]. By exploiting a hybrid configuration with lossy metal involved, the length of the polarizer can be reduced down to 30 μm, while maintaining a high extinction ratio (22 ~ 28 dB) and a moderate TE insertion loss (2 ~ 3 dB) [36]. Further reduction of the device footprint can be enabled through leveraging the mode cutoff in a silicon-based hybrid nanoplasmonic slot waveguide, which, however, comes at a price of degraded performance with a limited extinction ratio of around 16 dB [38]. A high-performance polarizer capable of striking a good balance between device footprint and optical performance has yet to be demonstrated.

Considering that the silicon-based hybrid $CaVO_3$ waveguide enables significantly different attenuations for different polarized modes, we exploit such a pronounced polarization dependent loss to develop an ultra-compact TE-pass polarizer at the telecommunication wavelengths, which is formed by integrating a hybrid vanadate configuration with a SOI platform. As shown schematically in Fig. 4, a $CaVO_3$-nanowire-loaded hybrid structure, featuring exactly the same geometry as that in Fig. 3, is connected with standard silicon ridge waveguides at both the input and output regions. A silica buffer layer is applied to cover over the entire SOI substrate in order to further minimize the coupling losses between different sections, which simultaneously acts as a low-index insulator gap facilitating the hybridization between different modes in the hybrid region. In the calculations, the lengths of both the input and output silicon waveguides are 1 μm, whereas the hybrid polarizer is 15 μm long. Parameters of the hybrid waveguide cross-section are the same as those in Fig. 3.

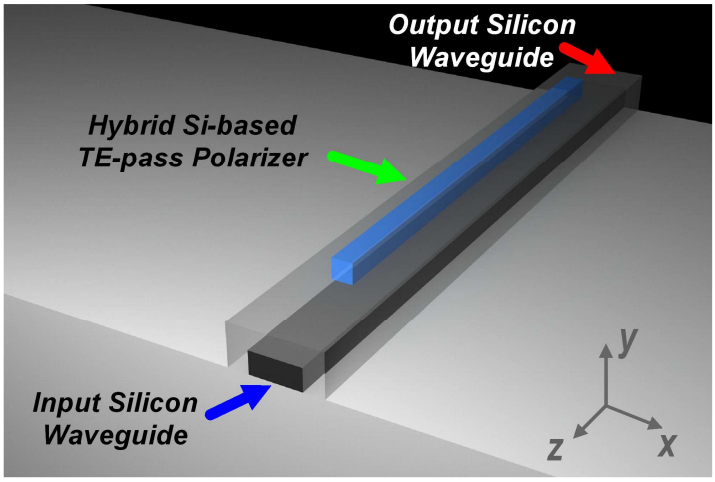

Fig. 4. Schematic of the proposed TE-pass polarizer integrated with silicon waveguides. The central region is a hybrid configuration that comprises a $CaVO_3$ nanowire placed on top of a silica-coated silicon ridge waveguide. The dimension of the hybrid waveguide is the same as that in Fig. 3. The dimensions of the polarizer are exactly the same as the input and output waveguides except the $CaVO_3$ nanowire. Other geometric parameters are the same as those in Fig. 3, which are obtained through optimizations in order to ensure low insertion loss, high extinction ratio and high efficiency excitation of the guided modes.

The optical performance of the polarizer is studied by employing 3D full-wave FEM simulations using COMSOL Multiphysics. Field evolution through the polarizer reveals the significantly different behavior of the TE- and TM-polarized modes, as illustrated in Fig. 5. For the TE polarization, the input silicon photonic mode remains almost unaffected by the presence of the $CaVO_3$ nanowire and experiences negligible attenuation through the device. In contrast, the input TM silicon photonic mode converts into a hybridized mode with a large attenuation, which decays dramatically along the propagation direction. This remarkable difference between the TE and TM insertion losses leads to an ultra-high extinction ratio of >30 dB at 1.55 μm. Performance comparisons shown in Table I indicate that our device features

simultaneously smaller footprint, higher extinction ratio and lower insertion loss, relative to the previously reported state-of-the-art hybrid TE-pass polarizer that incorporates a Cr nanowire. In addition, the back reflection of the proposed $CaVO_3$-based polarizer is below -60 dB, which is quite beneficial for maintaining the stability and reducing the laser noise for optical systems. The proposed TE-pass polarizer also performs well over a broad wavelength range, as revealed in Fig. 6. Enhanced extinction ratio and reduced insertion loss are observed when the working wavelength decreases. Low insertion losses (0.18 ~ 0.23 dB), together with high extinction ratios (22 ~ 34 dB), can be realized simultaneously within the wavelength range of 1.52 ~ 1.62 μm. Comparison with the polarizers built upon other materials such as ITO and transition metals further confirms the advantages of constructing a TE polarizer using vanadate materials (see S4 of the Supplementary Information for details).

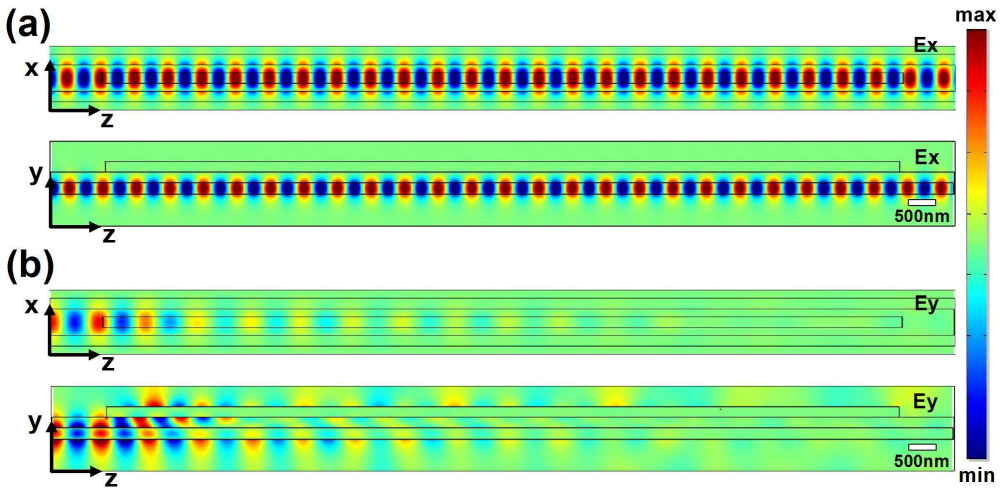

Fig. 5. Evolution of the electric fields for the (a) TE and (b) TM modes along the propagation direction through the polarizer at 1.55 μm within the x-z plane and y-z plane. The planes are cut along the centerlines of the Si waveguide.

TABLE I

Performance comparison between the proposed device and the hybrid TE-pass polarizer reported in [36] at 1.55 μm

Configuration	Proposed Device	Ref. [36]
Device Length (μm)	15	30
Extinction Ratio (dB)	30	26
TE Insertion Loss (dB)	0.19	2

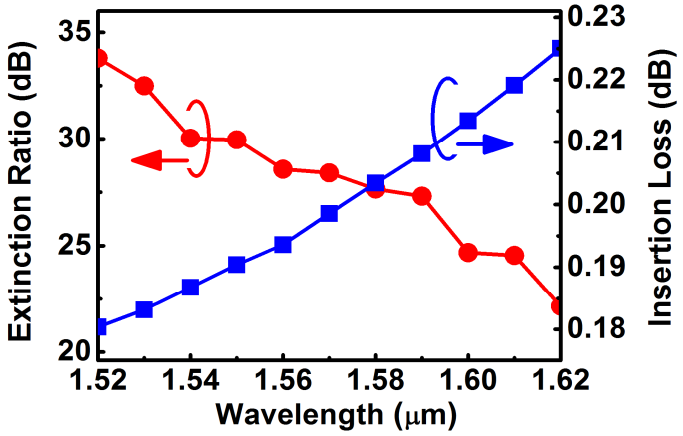

Fig. 6. Insertion loss and extinction ratio of the polarizer in the wavelength range of 1.52 ~ 1.62 μm.

The proposed TE polarizer can be fabricated based on a standard silicon-on-insulator substrate. After the formation of the silicon waveguide and the silica cladding, the vanadate layer can be deposited using hybrid molecular beam epitaxy [40, 41], followed by a patterning/etching process to define the nanowire. Considering the fabrication procedures for the hybrid TE-pass polarizer, it may be challenging to achieve high-precision alignment between the $CaVO_3$ nanowire and the silicon substrate, as well as the accurate control of the widths of the $CaVO_3$ nanowire and the silicon ridge waveguide. Further numerical studies are conducted to reveal the effect of these possible fabrication imperfections on the device performance, as shown in Fig. 7 and Table II. Clearly, despite the considered fabrication errors, the TE-pass polarizer maintains outstanding optical performance, demonstrating reasonable extinction ratios

(> 26.8 dB) and low insertion losses (< 0.32 dB). In addition, calculations indicate that such robust performance can be maintained over a broad wavelength range of 1.52 to 1.62 μm (See S3 of the Supplementary Information for details). The combined effect of all three considered fabrication errors are also studied and results show that high extinction ratios and low insertion losses can still be realized simultaneously under the considered wavelength range. These results clearly indicate that the overall properties of the TE-pass polarizer are quite robust against the considered fabrication imperfections, thus alleviating the fabrication requirement of high precision, which is certainly beneficial for their practical implementation.

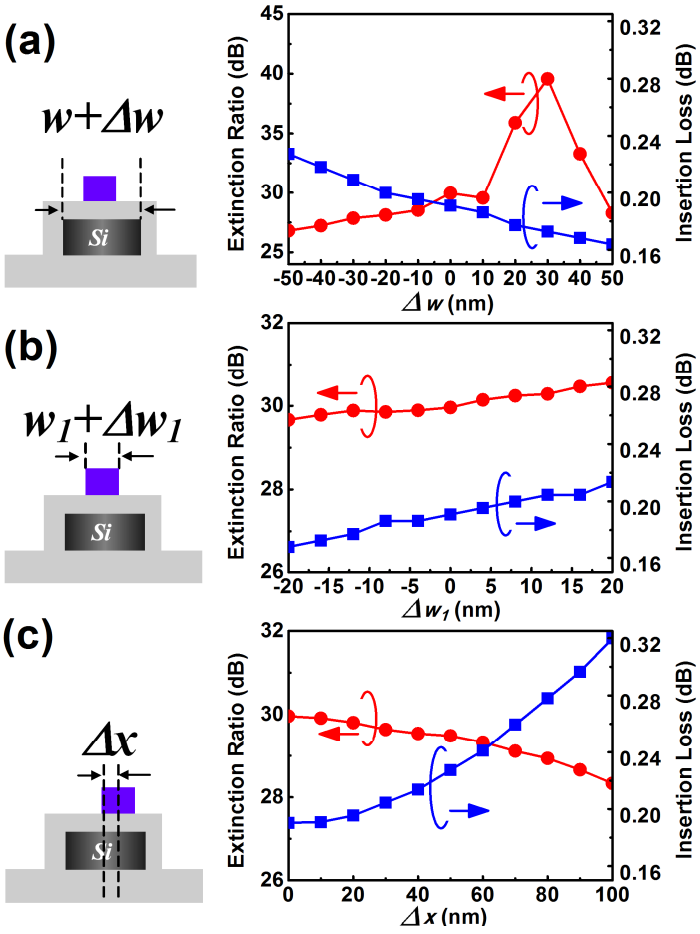

Fig. 7. Performance of the hybrid polarizer against possible fabrication imperfections: (a) variation

of the silicon ridge waveguide width (Δw); (b) variation of the $CaVO_3$ nanowire width (Δw_1); (c) lateral misalignment between the $CaVO_3$ nanowire and the silicon substrate (Δx).

TABLE II

Summary of the device performance against possible fabrication imperfections at the wavelength of 1.55 μm

Device (λ=1.55 μm)	Ideal Configuration	Fabrication Imperfection: Variation of Silicon Waveguide Width	Fabrication Imperfection: Variation of $CaVO_3$ NW Width	Fabrication Imperfection: Misalignment of $CaVO_3$ NW
ER (dB)	30	26.8~39.6	29.7~30.6	28.3~30
TE IL (dB)	0.19	0.164~0.227	0.168~0.214	0.19~0.319

4. Discussion

We have demonstrated that the integration of vanadate materials with typical waveguiding structures such as single interfaces and hybridized configurations, offers the possibility to further control the behavior of the optical guided modes. In addition to the waveguiding configurations considered here, the incorporation of vanadate structures in other well-investigated SPP platforms may also lead to interesting optical properties. For instance, traditional long-range SPP waveguides based on noble metals suffer from weak optical confinement, leading to significantly larger mode size than the operating wavelength [42]. Using vanadate thin films as an alternative could effectively reduce the area of the guided mode, while still being capable of maintaining an ultra-low propagation loss. The substitution of $CaVO_3$ ($SrVO_3$) for conventional metals such as gold and silver could also be beneficial for creating high-performance hybrid long-range waveguides, which are capable of providing an improved balance between confinement and loss, and enabling reduced crosstalk when compared to their traditional waveguiding counterparts [43]. In addition, similar to the wedge [44], channel [45] and slot plasmon polaritons [45, 46], complex $CaVO_3$ ($SrVO_3$) structures in the form of wedges,

grooves and slots, could enable even more pronounced local field enhancement and tighter optical confinement as compared to flat configurations. Further integration of such structures with the SOI platform may provide an alternative way to realize ultra-deep-subwavelength waveguides and related devices [47].

Besides the ultra-compact TE-pass polarizer discussed in our case studies, TM-pass polarizers are also made possible through leveraging the lateral coupling between silicon ridge waveguides and $CaVO_3$ ($SrVO_3$) nanostructures. Other types of polarization handing devices, such as polarization beam splitters, can be enabled as well through laterally integrating silicon ridges with hybrid $CaVO_3$ ($SrVO_3$) configurations. Desired functionalities can be readily achieved based on the careful engineering of the phase matching conditions between different guided modes in the system. In addition to various passive photonic components, high-performance active devices such as modulators can also be realized by integrating $CaVO_3$ ($SrVO_3$) with additional tunable materials, such as ITO and vanadium dioxide (VO_2) [48, 49]. For example, by replacing the metallic gold pad in the previously demonstrated ITO-based hybrid device [20] with a thin $CaVO_3$ film/nanowire, an ultra-compact modulator that features simultaneously enhanced optical performance and miniaturized device footprint can be enabled at the telecommunication wavelengths.

Since vanadate-based composites offer dramatically enhanced optical confinement, more significant local electromagnetic field enhancement, and considerably stronger light-matter interactions as compared to their conventional metal-based counterparts, it is expected that they also provide a pathway towards the realization of numerous other optical devices beyond those considered in this paper. For example, highly-efficient light concentrators capable of confining and storing optical energy within a

subwavelength space can be realized by embedding dielectric layers in between a multilayer $CaVO_3$ ($SrVO_3$) configuration [50]. Another important field that could benefit from vanadate materials is bio-chemical sensing [51]. By leveraging the strongly enhanced light-matter interactions in thin vanadate films and other complex vanadate nanostructures, significant amplification of the minute changes in the local environment could be enabled, thereby leading to high-performance bio-chemical sensors with ultra-high sensitivities.

5. Conclusion

In this work, through comprehensive numerical studies, we have revealed the unique guiding properties of the fundamental modes supported by several different types of configurations incorporating vanadate materials, including a single interface bounded by a $CaVO_3$ and dielectric layer, and hybridized structures integrating silicon waveguides and $CaVO_3$ substrate (nanowire). In contrast to traditional Ag-based configurations, waveguiding platforms involving $CaVO_3$ feature unique dispersion relationships within the near-infrared regime, facilitating enhanced local field confinement and stronger light-matter interactions. By exploiting the unique attenuation properties of a hybrid $CaVO_3$ waveguide (*i.e.* the polarization dependent loss), an ultra-compact TE-pass polarizer was proposed and numerically demonstrated based on a standard SOI platform. Results show that a device of 15 μm in length is capable of achieving a high extinction ratio of 22 ~ 34 dB, a low insertion loss of 0.18 ~ 0.23 dB, in conjunction with a good fabrication tolerance within the wavelength range of 1.52 ~ 1.62 μm, which clearly outperforms the current state-of-the-art in silicon polarizers. Our studies indicate that the exploitation of vanadate materials in waveguiding configurations provides a new route towards novel functional devices with miniaturized footprint and enhanced

performance. In addition, the manipulation of light at the deep-subwavelength scale using plasmonics can be complemented by these alternative materials, potentially opening up a new horizon for intriguing applications that would be otherwise difficult to realize with building blocks based on more traditional material systems.

Acknowledgements

This work was partially supported by the Penn State MRSEC, Center for Nanoscale Science, under the award NSF DMR-1420620.

References

1. J. D. Joannopoulos, P. R. Villeneuve and S. H. Fan, *Nature*, 1997, **386**, 143-149.
2. J. A. Schuller, E. S. Barnard, W. Cai, Y. C. Jun, J. S. White and M. L. Brongersma, *Nat. Mater.*, 2010, **9**, 193-204.
3. R. Soref, *IEEE J. of Quantum Electron.*, 2006, **12**, 1678-1687.
4. M. Lipson, *J. Lightwave Technol.*, 2005, **23**, 4222-4238.
5. W. L. Barnes, A. Dereux and T. W. Ebbesen, *Nature*, 2003, **424**, 824-830.
6. E. Ozbay, *Science*, 2006, **311**, 189-193.
7. C. L. Zhao, Y. M. Liu, Y. H. Zhao, N. Fang and T. J. Huang, *Nat. Commun*, 2013, **4**, 2305.
8. D. K. Gramotnev and S. I. Bozhevolnyi, *Nat. Photon.*, 2010, **4**, 83-91.
9. A. F. Koenderink, A. Alu and A. Polman, *Science*, 2015, **348**, 516-521.
10. R. Kirchain and L. Kimerling, *Nat. Photon.*, 2007, **1**, 303-305.
11. G. V. Naik, V. M. Shalaev and A. Boltasseva, *Adv. Mat.*, 2013, **25**, 3264-3294.
12. P. R. West, S. Ishii, G. V. Naik, N. K. Emani, V. M. Shalaev and A. Boltasseva, *Laser Photonics Rev.*, 2010, **4**, 795-808.
13. G. V. Naik and A. Boltasseva, *Phys. Status Solidi-RRL*, 2010, **4**, 295-297.
14. M. A. Noginov, L. Gu, J. Livenere, G. Zhu, A. K. Pradhan, R. Mundle, M. Bahoura, Y. A. Barnakov and V. A. Podolskiy, *Appl. Phys. Lett.*, 2011, **99**, 021101.
15. A. J. Freeman, K. R. Poeppelmeier, T. O. Mason, R. P. H. Chang and T. J. Marks, *Mrs Bulletin*, 2000, **25**, 45-51.
16. D. S. Ginley and C. Bright, *Mrs Bulletin*, 2000, **25**, 15-18.
17. B. G. Lewis and D. C. Paine, *Mrs Bulletin*, 2000, **25**, 22-27.
18. K. Ellmer, *Nat. Photon.*, 2012, **6**, 808-816.
19. E. Feigenbaum, K. Diest and H. A. Atwater, *Nano Lett.*, 2010, **10**, 2111-2116.
20. V. J. Sorger, N. D. Lanzillotti-Kimura, R.-M. Ma and X. Zhang, *Nanophotonics*, 2012, **1**, 17-22.
21. H. W. Lee, G. Papadakis, S. P. Burgos, K. Chander, A. Kriesch, R. Pala, U. Peschel and H. A. Atwater, *Nano Lett.*, 2014, **14**, 6463-6468.
22. X. G. Yu, T. J. Marks and A. Facchetti, *Nat. Mater.*, 2016, **15**, 383-396.
23. L. Zhang, Y. J. Zhou, L. Guo, W. W. Zhao, A. Barnes, H. T. Zhang, C. Eaton, Y. X. Zheng, M. Brahlek, H. F. Haneef, N. J. Podraza, M. H. W. Chan, V. Gopalan, K. M. Rabe and R. Engel-Herbert, *Nat. Mater.*, 2016, **15**, 204-211.
24. J. A. Dionne, L. A. Sweatlock, H. A. Atwater and A. Polman, *Phys. Rev. B*, 2005, **72**, 075405.
25. P. B. Johnson and R. W. Christy, *Phys. Rev. B*, 1972, **6**, 4370-4379.
26. R. F. Oulton, V. J. Sorger, D. A. Genov, D. F. P. Pile and X. Zhang, *Nat. Photon.*, 2008, **2**, 496-500.

27. R. F. Oulton, V. J. Sorger, T. Zentgraf, R. M. Ma, C. Gladden, L. Dai, G. Bartal and X. Zhang, *Nature*, 2009, **461**, 629-632.
28. V. J. Sorger, Z. Ye, R. F. Oulton, Y. Wang, G. Bartal, X. Yin and X. Zhang, *Nat. Commun.*, 2011, **2**, 331.
29. M. Z. Alam, J. S. Aitchison and M. Mojahedi, *Laser Photonics Rev.*, 2014, **8**, 394-408.
30. D. X. Dai and S. L. He, *Opt. Express*, 2009, **17**, 16646-16653.
31. T. Barwicz, M. R. Watts, M. A. Popovic, P. T. Rakich, L. Socci, F. X. Kartner, E. P. Ippen and H. I. Smith, *Nat. Photon.*, 2007, **1**, 57-60.
32. H. Fukuda, K. Yamada, T. Tsuchizawa, T. Watanabe, H. Shinojima and S. I. Itabashi, *Opt. Express*, 2008, **16**, 4872-4880.
33. D. Dai, J. Bauters and J. E. Bowers, *Light Sci. Appl.*, 2012, **1**, 1-12.
34. D. Dai, Z. Wang, N. Julian and J. E. Bowers, *Opt. Express*, 2010, **18**, 27404-27415.
35. Q. A. Wang and S. T. Ho, *IEEE Photon. J.*, 2010, **2**, 49-56.
36. X. Sun, M. Z. Alam, S. J. Wagner, J. S. Aitchison and M. Mojahedi, *Opt. Lett.*, 2012, **37**, 4814-4816.
37. M. Z. Alam, J. S. Aitchison and M. Mojahedi, *Opt. Lett.*, 2012, **37**, 55-57.
38. Y. Huang, S. Zhu, H. Zhang, T.-Y. Liow and G.-Q. Lo, *Opt. Express*, 2013, **21**, 12790-12796.
39. X. W. Guan, P. X. Chen, S. T. Chen, P. P. Xu, Y. C. Shi and D. X. Dai, *Opt. Lett.*, 2014, **39**, 4514-4517.
40. M. Brahlek, A. S. Gupta, J. Lapano, J. Roth, H. T. Zhang, L. Zhang, R. C. Haislmaier and R. Engel-Herbert, *Adv. Funct. Mater.*, 2018, **28**, 1702772.
41. C. Eaton, J. Lapano, L. Zhang, M. Brahlek and R. Engel-Herbert, *Journal of Vacuum Science & Technology A* 2017, **35**, 061510.
42. P. Berini, *Adv. Opt. Photonics*, 2009, **1**, 484-588.
43. Y. S. Bian and Q. H. Gong, *Appl. Phys. Lett.*, 2014, **104**, 251115.
44. E. Moreno, S. G. Rodrigo, S. I. Bozhevolnyi, L. Martin-Moreno and F. J. Garcia-Vidal, *Phys. Rev. Lett.*, 2008, **100**, 023901.
45. S. I. Bozhevolnyi, V. S. Volkov, E. Devaux, J. Y. Laluet and T. W. Ebbesen, *Nature*, 2006, **440**, 508-511.
46. J. A. Dionne, L. A. Sweatlock, H. A. Atwater and A. Polman, *Phys. Rev. B*, 2006, **73**, 035407.
47. Y. S. Bian and Q. H. Gong, *Laser Photonics Rev.*, 2014 **8**, 549-561.
48. L. Liu, L. Kang, T. S. Mayer and D. H. Werner, *Nat. Commun.*, 2016, **7**.
49. H. T. Zhang, L. Zhang, D. Mukherjee, Y. X. Zheng, R. C. Haislmaier, N. Alem and R. Engel-Herbert, *Nat. Commun.*, 2015, **6**, 8475.
50. N. N. Feng, J. Michel and L. C. Kimerling, *IEEE J. of Quantum Electron.*, 2006, **42**, 885-890.
51. J. Homola, S. S. Yee and G. Gauglitz, *Sens. Actuators B Chem.*, 1999, **54**, 3-15.

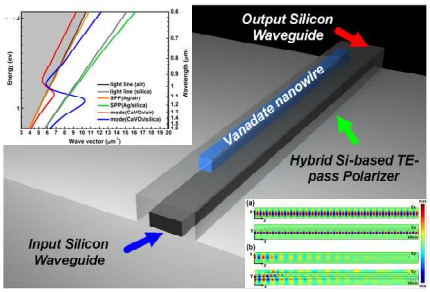

The integration of vanadate materials with planar waveguiding platforms enables novel functional devices with miniaturized footprint and enhanced performance